


Original research

Mutations in *VWA8* cause autosomal-dominant retinitis pigmentosa via aberrant mitophagy activation

Linghui Kong,¹ Guoming Chu,² Wei Ma,¹ Jiajian Liang,³ Dan Liu,¹ Qiushi Liu,⁴ Xiaowei Wei,¹ Shanshan Jia,¹ Hui Gu,¹ Yiwen He,¹ Wenting Luo,¹ Songying Cao,¹ Xiaomeng Zhou,⁵ Rong He,² Zhengwei Yuan ¹

► Additional supplemental material is published online only. To view, please visit the journal online (<http://dx.doi.org/10.1136/jmg-2022-108888>).

¹Key Laboratory of Health Ministry for Congenital Malformation, Department of Pediatric Surgery, Shengjing Hospital of China Medical University, Shenyang, Liaoning, China

²Department of Clinical Genetics, Shengjing Hospital of China Medical University, Shenyang, Liaoning, China

³Department of Orthopedic Surgery, Shengjing Hospital of China Medical University, Shenyang, Liaoning, China

⁴Department of Ophthalmology, Fourth People's Hospital of Shenyang, Shenyang, Liaoning, China

⁵MyGenostics Inc, Beijing, China

Correspondence to

Dr Zhengwei Yuan, Key Laboratory of Health Ministry for Congenital Malformation, Department of Pediatric Surgery, Shengjing Hospital of China Medical University, Shenyang, Liaoning 110004, China; yuanzw@hotmail.com
Dr Rong He; her@sj-hospital.org

LK and GC contributed equally.

Received 23 August 2022
Accepted 20 March 2023



© Author(s) (or their employer(s)) 2023. No commercial re-use. See rights and permissions. Published by BMJ.

To cite: Kong L, Chu G, Ma W, et al. *J Med Genet* Epub ahead of print: [please include Day Month Year]. doi:10.1136/jmg-2022-108888

ABSTRACT

Background Although retinitis pigmentosa (RP) is the most common type of hereditary retinal dystrophy, approximately 25%–45% of cases remain without a molecular diagnosis. von Willebrand factor A domain containing 8 (*VWA8*) encodes a mitochondrial matrix-targeted protein; its molecular function and pathogenic mechanism in RP remain unexplained.

Methods Family members of patients with RP underwent ophthalmic examinations, and peripheral blood samples were collected for exome sequencing, ophthalmic targeted sequencing panel and Sanger sequencing. The importance of *VWA8* in retinal development was demonstrated by a zebrafish knockdown model and cellular and molecular analysis.

Results This study recruited a Chinese family of 24 individuals with autosomal-dominant RP and conducted detailed ophthalmic examinations. Exome sequencing analysis of six patients revealed heterozygous variants in *VWA8*, namely, the missense variant c.3070G>A (p.Gly1024Arg) and nonsense c.4558C>T (p.Arg1520Ter). Furthermore, *VWA8* expression was significantly decreased both at the mRNA and protein levels. The phenotypes of zebrafish with *VWA8* knockdown are similar to those of clinical individuals harbouring *VWA8* variants. Moreover, *VWA8* defects led to severe mitochondrial damage, resulting in excessive mitophagy and the activation of apoptosis.

Conclusions *VWA8* plays a significant role in retinal development and visual function. This finding may provide new insights into RP pathogenesis and potential genes for molecular diagnosis and targeted therapy.

INTRODUCTION

Retinitis pigmentosa (RP, MIM 268000) is the most common hereditary retinal dystrophy that affects 1 in 4000 individuals worldwide.¹ RP is genetically heterogeneous and can be inherited as an autosomal-dominant (ad) (30%–40%), autosomal-recessive (50%–60%) and X-linked-recessive (10%–15%) trait.² Presently, there is no effective treatment for preventing the development and progression of RP or restoring the function of cones and rods; existing pharmacological agents can only delay the progression of RP through neuroprotection.^{3–4} However, antisense oligonucleotide (ASO) technology and gene-based therapy have shown promising results in

WHAT IS ALREADY KNOWN ON THIS TOPIC

⇒ Although more than 24 genes and loci have been identified in non-syndromic autosomal-dominant retinitis pigmentosa (RP), quite part of cases remain without a molecular diagnosis. The genetic diagnosis and pathogenesis of specific cases remain in need of further research, which could help identify potential therapeutic targets.

WHAT THIS STUDY ADDS

⇒ Our study found variant c.3070G>A; c.4558C>T (p.Gly1024Arg; p.Arg1520Ter) in von Willebrand factor A domain containing 8 (*VWA8*) linked to retinal diseases, identified that *VWA8* plays an important role in mitophagy and apoptosis, which enriches the study of its molecular function, and provides a reference for subsequent *VWA8*-related studies.

HOW THIS STUDY MIGHT AFFECT RESEARCH, PRACTICE OR POLICY

⇒ Our study fills the blank of the *VWA8* expression map in eye tissue, paving the way for future research on the specific roles of *VWA8* in ophthalmic diseases. *VWA8* could be a key molecule for RP prenatal screening and a potential therapeutic target for RP treatment and provides a reference value for the study of other neurodegenerative diseases.

treating RP.⁵ PR1123 (previously named ION357) is an ASO drug that targets the P23H variant in the human *RHO* gene and has shown an effective treatment strategy.^{6,7} However, RP is highly heterogeneous, and more than 24 genes and loci have been identified in non-syndromic autosomal-dominant Retinitis Pigmentosa (adRP) (RetNet). Although considerable progress has been made in identifying adRP genes and pathogenic variants owing to the development of targeted next-generation sequencing, approximately 25%–45% of cases remain without a molecular diagnosis.^{8,9} These findings emphasise the need for setting a genetic diagnosis for specific cases and investigating the pathogenic mechanism which might help with the discovery of potential therapeutic targets.

Although it has been reported that the pathogenesis of RP is accompanied by oxidative damage in photoreceptors and retinal pigment epithelial cells, the exact mechanism has not yet been elucidated.¹⁰ Photoreceptor homeostasis is maintained by a dynamic equilibrium between autophagy and apoptosis. Autophagy is a beneficial process in most cases, in which autophagosomes fuse with lysosomes to degrade impaired cytoplasmic components and reduce apoptosis to maintain cell homeostasis.¹¹ Mitophagy is a selective form of macroautophagy in which dysfunctional and damaged mitochondria can be efficiently degraded, removed and recycled through autophagy.¹² Studies have shown that adRP-related genes, including *PRPF8*, *PRPF6*, *PRPF31* and *SNRNP200*, interfere with the initiation of hypoxia-induced mitophagy by impeding proper mRNA splicing of unc-51 like autophagy activating kinase 1 (*ULK1*), resulting in defective regulation of mitophagy,¹³ indicating that appropriate autophagic flux in photoreceptors may be beneficial. Aberrantly hyperactivated mitophagy could be deleterious and may ultimately lead to cell death.^{14–16} Conditional knockout of ubiquitously expressed prefoldin-like chaperone (*UXT*) was found to induce retinal degeneration and pigmentation in mice by boosting autophagic flux and apoptosis.¹⁷ However, the cross-regulation between apoptosis and autophagy is yet to be understood, with further studies being needed to clarify their relationship, which may shed light on the mechanism of photoreceptor cell death in some cases of RP. von Willebrand factor A domain containing 8 (*VWA8*, MIM 617509), also named KIAA0564, encodes a mitochondrial matrix-targeted protein with three ATPase-associated domains and a von Willebrand factor A domain associated with ATPase activity.^{18–19} Previous studies have linked *VWA8* to autism,²⁰ bipolar disorder, comorbid migraine, variation in corpus callosum size,^{21–22} developmental delay, microcephaly and scoliosis.²³ Some studies have also included *VWA8* into the candidate genes of multisystem inflammatory syndrome in children and familial autoimmunity.^{24–25} However, no study has implicated *VWA8* in retinal disease. Luo *et al*'s study showed that conditional deletion of *VWA8* in mouse liver cells can lead to increased mitochondrial compensatory and oxidative capacity,²⁶ suggesting *VWA8* may be related to energy metabolism. However, the specific effect and mechanism of *VWA8* deletion on mitochondrial function remains to be studied.

Here we report the identification of a heterozygous two-loci variant in *VWA8* in 24 individuals with adRP from a Chinese family by using exome sequencing and bioinformatics analysis. *VWA8* expression was reduced as a result of the premature termination of translation. The variant responsible for this loss of function in *VWA8* was found to be c.3070G>A;c.4558C>T (p.Gly1024Arg; p.Arg1520Ter). *VWA8* was specifically expressed in the retina of eye tissues. The downregulation in *VWA8* expression could lead to a similar RP phenotype with a narrowing of the photoreceptor layer and an abnormal response to dark adaptation in zebrafish, and the possible mechanism was explored in *VWA8*-deficient ARPE-19 cells. Our findings identify a new disease gene underlying adRP and provides insight into the mechanism of *VWA8* dysfunction.

MATERIALS AND METHODS

Patients

Fundus examinations were performed on each patient to diagnose the disease and assess its severity. Relevant tests were conducted and found no clinical symptoms associated with syndromic RP.

Experimental animals

Zebrafish (*Danio rerio*) wild-type strain Tübingen (TU) was obtained from Nanjing YSY Biote (Nanjing, China). The fish were maintained according to the national and international guidelines for the care and use of laboratory animals. All zebrafish studies were conducted under the guidance and approval of the Institutional Animal Care and Use Committee of the China Medical University.

Ophthalmic targeted sequencing panel

Microarray capture high-throughput sequencing of approximately 1 µg of peripheral blood genomic DNA for approximately 790 eye disease genes was performed on all individuals except I1, I4, I9, I13 and I14 to screen for known disease-causing gene variants (online supplemental table S1).

Exome sequencing and analysis

Peripheral blood samples of patients labelled with a blue asterisk (figure 1A) were collected for exome sequencing. The whole-exome region of the library was enriched using the Whole Exome Capture Kit (MyGenostics, Beijing, China)²⁷ according to the manufacturer's instructions. Sequencing of the captured libraries was performed on an Illumina NovaSeq 6000 (Illumina, San Diego, California, USA) with 150bp paired-end reads, according to the manufacturer's protocol. The reads were mapped to the hg19 human reference sequence (GRCh37). As for CNV calling, the total bases for each coding region were calculated using SAMtools, and the average mean depth of the consensus coding sequence (CCDS) regions was obtained by using the GATK 'DepofCoverage' command. The programme 'R' was used to calculate the ratio of each sample compared with the average ratio of the other samples, and the ggplot package was used to visualise the results. Ratios >1.4 were designated as duplicates, and those <0.6 were designated as deletions. Dely V.0.8.6 software was used to detect structure variants (SVs) and annotation mutations with table_annoar.pl (annoar_2020). SVs that meet the frequency of normal people and genes involved in SV related to RP were included as candidate variants. Finally, its accuracy was verified through bam map. The pathogenicity index of the identified variant was calculated using different online tools, such as PolyPhen-2, Mutation Taster, SIFT, Revel, splice AI, Mutation Assessor and Clinvar (detailed methods are shown in the online supplemental material). The frequency of the identified variants in the general population was calculated using ExAC/gnomAD, ESP6500 and 1000 Genomes Projects.

Sanger sequencing

Bidirectional Sanger sequencing was performed to confirm the *VWA8* and *SOX11* variants identified by next-generation sequencing, using specific oligonucleotide primers flanking exons (primer sequences: c.3070G>A (p.Gly1024Arg): F_TCATGACTGTGGCATCTGGA, R_GGCTGTGAC-CATTTTCAGAC; c.4558C>T (p.Arg1520Ter): F_GCAACTCA GTTTTGTAGAATGGA, R_TGAGCAAACACTGAAAGGGA; c.712delA: F_TGGGTTTATCAAGCCAATGTG, R_GCTC TCACAAATGTGGTGCTC).

VWA8 knockdown in zebrafish

Morpholinos (MOs) were synthesised using Gene Tools (Corvallis, Oregon, USA). The antisense sequence (25 bases) of the MO targeting the splice site of the *VWA8* gene corresponded to that between the six introns and seven exons of the coding region (*VWA8*-MO, 5'-AGCTGGTCCCTTAACATAAAAAACAGA-3')

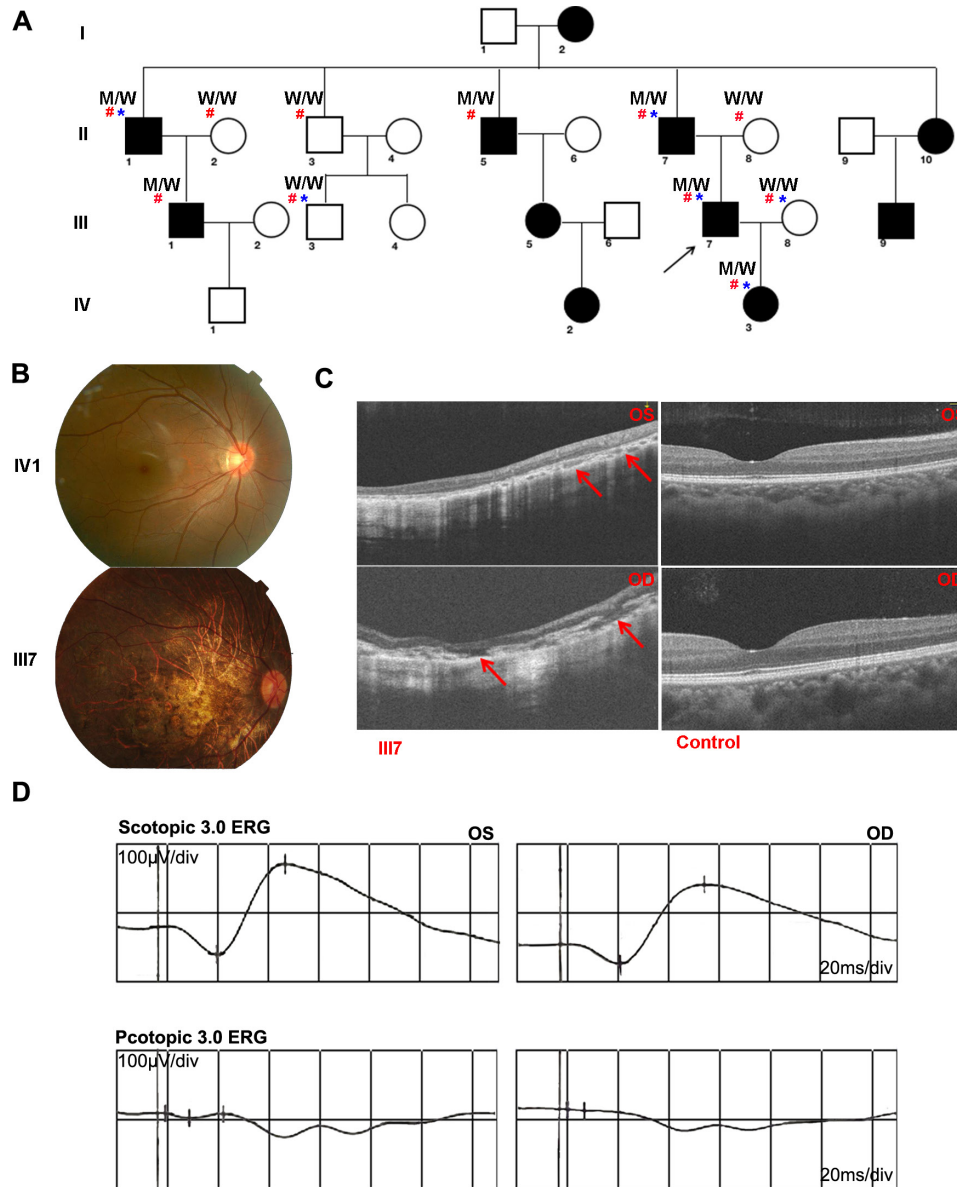


Figure 1 Clinical adRP families and individuals. (A) Pedigrees of families with segregating heterozygous *VWA8* loss-of-function variants. The identified heterozygous variants are shown for the 11 affected individuals, and the black arrow indicates the proband. Patients marked with blue asterisks provided peripheral blood for exome sequencing, and patients with red hashtags provided peripheral blood for Sanger sequencing. (B) Fundus photographs of the OD of individual III7 demonstrated severe thinning of the retinal arterioles, the presence of bone spicule-type pigment deposits in the peripheral retina and extensive retinal atrophy in the central area of the macula. The fundus images of unaffected individual IV1 were used as a control. (C) OCT scan of individual III7 shows a discontinuous retinal structure with large spots of retinal atrophy and a loss of volume of the ONL (red arrows); normal OCT images are shown as controls. (D) The proband patient exhibited a decreased response to scotopic 3.0 and photopic 3.0, and the scale bar indicates 100 μ V vertically and 20 ms horizontally. ERG, electroretinogram; M, mutant type; OCT, optical coherence tomography; OD, right eye; ONL, outer nuclear layer; OS, left eye; *VWA8*, von Willebrand factor A domain containing 8; W, wild type.

and control (control-MO, 5'-CCTCTTACCTCAGTTACAAT TTATA-3'). The MOs were injected into one to two cell stage zebrafish embryos. Agarose gel electrophoresis was performed on RT-PCR products, and 684 and 324 bp bands were sequenced to match the *VWA8* target sequence. Primer sequences of *VWA8*-MO were 5'-3' *VWA8*-MO_F: GAACACACTAAAGAAGAGCT and *VWA8*-MO_R: CAGAACAGTAAGGGCTGATG.

Light-Induced locomotor response

Larvae at 5 days post fertilisation (dpf) that had been injected with *VWA8*-MO or control MO were placed in a six-well plate. Larval behaviour was assessed using Viewpoint Zebralab3

(ViewPoint Life Sciences, Lyon, France). The larvae adapted to visible light at an intensity similar to that of the laboratory fluorescent lamp within 30 min. After the adaptation period, the locomotor response, calculated as the average swimming speed per minute, was recorded. The light cycle was 10 min of visible light, followed by 10 min of darkness, which was repeated for 50 min. Each photomotor experiment was performed on six fish per group.

RNA sequencing

Total RNA was extracted from ARPE-19 cells transfected with *VWA8*-siRNA or the appropriate controls. RNA concentration

and purity were determined using an Agilent 2100 Bioanalyzer (Agilent RNA 6000 Nano Kit, USA) and NanoDrop spectrophotometer, respectively. The transcriptome product combined poly(A)-selection of mRNA transcripts with a strand-specific cDNA library preparation, with a mean insert size of 250–300 bp. Libraries were sequenced on an Illumina Novaseq 6000 (Illumina). An index of the reference genome was built using hisat2-2.0.4, and paired-end clean reads were mapped against the reference genome. STAR used the method of maximal mappable prefix to generate a precise mapping result for junction reads. Each sample contained more than 12.08 G of data. Quality control was performed on the raw reads to determine whether the sequencing data fit the follow-up analysis.

Bioinformatic analysis

Differentially expressed genes (DEGs) were identified using DESeq2 V.1.4.5 at a p value of ≤ 0.05 . To gain insight into potential functions, gene set enrichment analysis (GSEA) was performed to identify enriched biological pathways by the set of genes between ARPE-19 cells transfected with *VWA8*-siRNA and appropriate controls. The Normalised Enrichment Score (NES) and nominal (NOM) p value were used to estimate the significantly enriched gene sets.

RT-qPCR analysis

Briefly, followed by cDNA synthesis from 2 μ g RNA, using TaKaRa RNA PCR kit (Takara, Tokyo, Japan). RT-PCR amplifications were performed in triplicate using a LightCycler 480 Instrument (Roche, Mannheim, Germany) with the following primers: 5'–3' *VWA8*_F: AAATGAGTGAATACGATGCTGC; *VWA8*_R: TCCAGTAGCTTGATGTCTTAGC); 5'–3' *VWA8*-3070-F:

TCCGACTGAAGGTCTCTCCA; *VWA8*-3070-R: ATCCCCTTCTTGCCTGACC; *VWA8*-4558-F: TGGCTGTCGACCATTTCAGA; *VWA8*-4558-R: AGGCATGTTGTCTGGGTCCT. The relative mRNA levels of each sample were calculated according to the $2^{-\Delta\Delta Ct}$ method, using glyceraldehyde-3-phosphate dehydrogenase (*GAPDH*) expression for normalisation.

Western blotting analysis

Total protein was extracted using radioimmunoprecipitation buffer (Solarbio Science & Technology, Beijing, China). Thereafter, the proteins were transferred into membranes and incubated with primary antibodies overnight at 4°C. The primary antibodies included anti-LC3 (1:1000, Abcam), anti-P62 (1:2000, ProteinTech, China), anti-GAPDH (1:5000, ProteinTech), anti-*VWA8* (1:5000, Novus), anti-cytochrome C (1:1500, Cell Signal Technology), anti-Cox IV (1:2000, Cell Signal Technology), anti-Bcl-2 (1:1000, Cell Signal Technology), anti-Bax (1:2000, Cell Signal Technology), anti-caspase 3 (1:2500, Novus) and anti-caspase 9 (1:200, 0Cell Signal Technology). Subsequently, membranes were incubated with the corresponding secondary antibodies (1:5000, ProteinTech) at room temperature for 1 hour. The proteins were visualised with enhanced chemiluminescence reagent (Millipore, Billerica, Massachusetts, USA).

Statistical analysis

Statistical analyses were performed using GraphPad Prism V.8 (GraphPad Software), and all data are presented as mean \pm SE of the mean. Statistical comparison between the two groups was performed using Student's t -test, whereas multiple comparisons among three or more groups were performed using one-way

analysis of variance. Statistical differences in light-induced locomotor response were determined using Dunnett's test.

RESULTS

Clinical phenotype

A Chinese family consisting of 24 members was screened for adRP (figure 1A), among which 11 were affected, according to the results of detailed clinical examination and fundus photography. The ages of the patients ranged from 9 years to 87 years, and all the patients presented initial symptoms of night blindness and visual field defects (online supplemental figure S1) and reduced visual acuity later. The onset age varied from early childhood to 12 years of age (online supplemental table S2), and all patients had macular changes, including macular degeneration and dystrophy (online supplemental figure S1). Additionally, the best-corrected visual acuity (BCVA) of patients II5 and III7 was 0.1 and 0.4 for IV3. Blood lipid tests showed that patients II7, II10, III5, III7 and IV2 had abnormal blood lipid parameters. Notably, patients III7 and IV2 showed significant signs of obesity, without bone or heart developmental problems (online supplemental table S2). III7 is the proband of the family (figure 1A, black arrow), exhibiting thinning of the retinal arterioles, presence of bone spicule-type pigment deposits in the peripheral retina and extensive retinal atrophy in the central area of the macula (figure 1B). Additionally, optical coherence tomography showed a discontinuous retinal structure with large spots of retinal atrophy and a loss of volume in the outer nuclear layer (photoreceptor layer, red arrows) (figure 1C). Moreover, electroretinogram analysis (figure 1D) confirmed adRP in the patients.

Exome sequencing detected a variant of *VWA8*

The patients were screened for variants in 790 genes related to eye diseases to identify potential genetic defects responsible for adRP; however, no variant was observed. Therefore, exome sequencing of four patients and two unaffected subjects was performed, using Novaseq 6000 sequencer (Illumina) (figure 1A, blue asterisks). The average sequencing depth and coverage were 206.43 and 99.58%, respectively, and the percentage of regions with sequencing depth of >20 was 98.28%. Compared with unaffected subjects, 1560 suitable genetic separation loci were screened from a total of 95 510 loci. Subsequently, 120 loci with the highest minor allele frequency of ≤ 0.001 or loci absent from the normal population were selected. We excluded loci located in deep intron region with a splice AI score of less than 0.5 (online supplemental table S3) and unknown loci located in the untranslated region (UTR) region, which have not been reported in the literature, and synonymous loci were removed, after which 39 variants including missense mutation, splicing mutation, frameshift mutation and nonsense mutation were retained (online supplemental table S4). Furthermore, seven sites with variants that severely affect protein function, including splicing, frameshift and nonsense variants, were selected (online supplemental table S5). Four loci were retained in four genes (*VWA8*, *KLHL17*, *STOX1* and *NBEAL1*) by eliminating variation in non-standard transcripts. *STOX1* has been shown to be associated with pre-eclampsia, PEE4 (MIM 609404),²⁸ and the variant c.712delA was validated not completely segregated with adRP by Sanger sequencing (online supplemental figure S2). Then SpliceAI predicted that *KLHL17* and *NBEAL1* might be non-functional splicing mutations, and we considered SpliceAI score of ≥ 0.5 as candidate pathogenic mutations. Therefore, we targeted the candidate pathogenic variant in *VWA8*. The variant

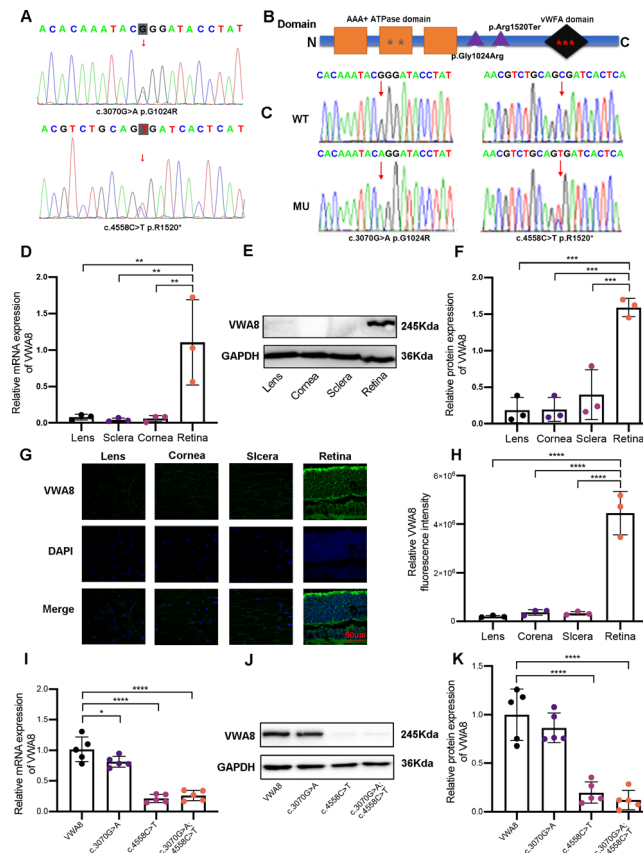


Figure 2 Sanger sequencing and function of *VWA8* variants. (A) Sanger sequencing identified that the proband carried two heterozygous *VWA8* variants. c.3070G>A (p.Gly1024Arg) is a 1 bp missense mutation, while c.4558C>T (p.Arg1520Ter) is a nonsense mutation. The nucleotide sequence is shown on each chromatogram. (B) Schematic representation of the *VWA8* domains (1905 amino acids) contains three predicted ATPase, dynein-related, AAA domains (orange boxes) with the second AAA domain containing an ATPase binding site bounded by the Walker A and Walker B (two grey asterisks) motifs. *VWA8* has a predicted von Willebrand factor type A domain (black diamond) at the C-terminus containing a MIDAS noted by red asterisks. (C) Sequencing of the products of the WT group and c.3070G>A and c.4558C>T (p.Gly1024Arg and p.Arg1520Ter) group reveals the existence of the c.3070G>A and c.4558C>T (p.Gly1024Arg and p.Arg1520Ter) variant at the mRNA level. (D) RT-qPCR analysis of three normal fetal eyes revealed high expression of *VWA8* in the human retina and low expression in the cornea, sclera and lens (n=3, ANOVA). (E) Representative western blot of the retina, cornea, sclera and lens of fetal eye tissues for *VWA8* expression. GAPDH was used as a loading control. (F) Histogram showing the relative expression of *VWA8* protein in the retina, cornea, sclera and lens of fetal eye tissues. The retina had a higher expression of *VWA8* protein compared with the other eye tissues. Data are presented as the mean±SD of the densitometry intensity of each lane in three independent experiments, which were normalised to GAPDH (n=3, ANOVA). (G) Immunofluorescence staining of the retina, cornea, sclera and lens of fetal eye tissues for *VWA8* (green), and cell nuclei were counterstained with 4',6-diamidino-2-phenylindole (DAPI) (blue). Scale bar=50 µm. (H) Histogram showing the relative fluorescence intensities of the retina, cornea, sclera and lens of fetal eye tissues for *VWA8*. *VWA8* was highly expressed in the retina but hardly expressed in other eye tissues. Data are presented as the mean±SD of three independent experiments (n=3, ANOVA). (I) RT-qPCR analysis of 293T cells transfected with three *VWA8* MU plasmids, including c.3070G>A (p.Gly1024Arg), c.4558C>T (p.Arg1520Ter), and c.3070G>A and c.4558C>T (p.Gly1024Arg and p.Arg1520Ter). Transfection with plasmids containing c.4558C>T (p.Arg1520Ter) or c.3070G>A and c.4558C>T (p.Gly1024Arg and p.Arg1520Ter) significantly reduced *VWA8* mRNA levels in 293T cells, whereas only a slight decrease in *VWA8* mRNA level was observed in cells transfected with c.3070G>A (p.Gly1024Arg) (n=5, ANOVA). (J) Representative western blot of 293T cells transfected with three *VWA8* MU plasmids; GAPDH was used as a loading control. (K) Histogram showing the relative expression of *VWA8* protein in 293T cells transfected with three different types of *VWA8* MU plasmids. Transfection with c.4558C>T (p.Arg1520Ter) or c.3070G>A and c.4558C>T (p.Gly1024Arg and p.Arg1520Ter) plasmids induced only a slight expression of *VWA8* protein. Data are presented as the means±SD of the intensity of each lane in five independent experiments, which were normalised to GAPDH (n=5, ANOVA). *P<0.05, **P<0.01, ***P<0.001, ****P<0.0001. ANOVA, analysis of variance; MIDAS, metal ion-dependent adhesion site; MU, mutant; *VWA8*, von Willebrand factor A domain containing 8; WT, wild type.

was validated segregate with adRP by Sanger sequencing of six patients and five normal subjects (figures 1A and 2A). These findings suggest that this is a potentially pathogenic variant. Furthermore, RT-qPCR and western blotting analysis were performed on the retina, cornea, lens and sclera of the eyes of fetuses 30–35 weeks old (most of the retina is already developed at 30 weeks^{29 30}) to determine the spatial expression of *VWA8*. Compared with other parts of the eyes, the retina had a higher expression of *VWA8* at both mRNA and protein levels

(figure 2D–F), which was confirmed by immunofluorescence staining (figure 2G,H). These results suggest that *VWA8* plays an important role in retinal development.

Although there is no suitable tertiary structure model to predict changes in structure resulting from the variant c.4558C>T (p.Arg1520Ter), all 38–45 exons were lost after the mutation, suggesting the production of truncated proteins, among which the missing region (1712–1901 region) is the vWFA domain. However, the mutation c.3070G>A (p.Gly1024Arg) was

not located in the critical domain (figure 2B). Therefore, we hypothesised that c.3070G>A; c.4558C>T (p.Gly1024Arg; p.Arg1520Ter) could be a 'loss of function' variant of *VWA8*. Three plasmids with the *VWA8* missense mutation and a wild-type plasmid were constructed and transfected into 293T cells using liposomes. Compared with cells transfected with the wild-type plasmid, 293T cells transfected with plasmids containing the variants (c.4558C>T (p.Arg1520Ter) and c.3070G>A; c.4558C>T (p.Gly1024Arg; p.Arg1520Ter)) had significantly lower *VWA8* expression levels both at the mRNA and protein levels (figure 2I–K). Then, the PCR products of the wild-type group and the c.3070G>A; c.4558C>T (p.Gly1024Arg; p.Arg1520Ter) group were sequenced. Sequencing results showed that there was a truncated variant at the mRNA level (figure 2C), indicating that mRNA containing the variant may have the capacity to escape nonsense-mediated decay (NMD). Meanwhile, 293T cells transfected with the p.Gly1024Arg; p.Arg1520Ter plasmid showed similar dysfunction as *VWA8*-siRNA transfected cells including abnormal autophagy activation and apoptosis activation (online supplemental figure S3). Collectively, our data suggested that the p.Gly1024Arg; p.Arg1520Ter variant of *VWA8* is more likely a loss of function mutation in the sense of downregulation in the expression of *VWA8*, leading to abnormal autophagy and apoptosis activation. Notably, although c.3070G>A (p.Gly1024Arg) and c.4558C>T (p.Arg1520Ter) are inherited together, the variant c.4558C>T (p.Arg1520Ter) may be more involved in downregulating *VWA8* expression than the variant c.3070G>A (p.Gly1024Arg).

Vwa8 knockdown induced visual impairment in zebrafish

Vwa8 knockdown zebrafish model was developed to verify whether the loss of *Vwa8* function can cause RP by microinjecting zebrafish embryos (one to two cell stage) with MOs targeting the splice sites of the *Vwa8* gene (figure 3A). Compared with embryos injected with control MO, knocking down *Vwa8* significantly reduced *Vwa8* expression from 2 dpf to 5 dpf (figure 3B and online supplemental figure S3). Sanger sequencing of RT-PCR products amplified with *Vwa8*-MO primers in each period (2, 3, 4 and 5 dpf) matched the *Vwa8* gene sequence, confirming that the *Vwa8* knockdown model was successfully constructed (online supplemental figure S4). Additionally, knocking down *Vwa8* induced abnormal phenotypes, including retinal pigment deposition (figure 3C), eyes with damaged photoreceptor cells and severe malformation, with significantly higher fetal mortality and morbidity in 57.3% of fish (total number of examined fish was 75) compared with embryos in the control group (online supplemental table S6). In contrast, 95.8% of fish (n=72) injected with the control MO exhibited a normal phenotype (online supplemental table S6). Additionally, there was a significant narrowing of the retinal photoreceptor layer in *Vwa8*-knockdown larvae 5 dpf (figure 3D). These results suggest that knocking down *Vwa8* can cause an abnormal retinal phenotype in zebrafish. Furthermore, we assessed the swimming response of 5 dpf larvae to sudden light-to-dark transitions to determine the effect of *Vwa8* knockdown on visual function. Behavioural analysis showed that 5 dpf larvae with low *Vwa8* expression levels exhibited aberrant locomotor response during the light-off phase (figure 3E,F).

Transcriptome alterations in *VWA8*-deficient ARPE-19 cells

VWA8 was knocked down in ARPE-19 cells by siRNA interference to explore the mechanism of *VWA8* in RP. To exclude the influence of biological interference, two siRNAs were selected

for validation by several assays (online supplemental figure S5). RNA-Seq was used to identify DEGs between control ARPE-19 cells and *VWA8*-siRNA transfected cells. A total of 158 upregulated and 136 downregulated DEGs were identified in the siRNA versus control groups (figure 4A). We used GSEA V3.0 software for GSEA analysis; all enriched pathways associated with cellular processes, and the top 10 significantly enriched terms ($p < 0.05$ and $|NES| > 1$) in biological processes (BPs) and cellular components (CCs) are shown in figure 4. The most enriched KEGG pathways were apoptosis, necroptosis, autophagy, mitophagy, P53 signalling pathway and lysosomes (figure 4B). The most enriched terms in BP were mitochondria-related terms, including mitochondrial transport; apoptosis-related terms, including regulation of the stat cascade, intrinsic apoptotic signalling pathway by P53 class mediator and striated muscle cell apoptotic process; and autophagy-related terms, including lysosome localisation (figure 4C). The most enriched terms in CC were mitochondria-related terms, including the extrinsic component of organelle membrane, ATPase-dependent transmembrane transport complex, and cation-transporting ATPase complex and apoptosis-related terms, including telomerase holoenzyme complex (figure 4D). Enrichment plots from the GSEA analysis of autophagy, apoptosis and mitochondrial transport are presented in figure 4E. Overall, these results suggest that the role of the *VWA8* variant in RP may be related to abnormal mitochondrial function, autophagy and apoptosis.

Decrease in *VWA8* expression induced mitophagy

Furthermore, we clarified whether downregulation of *VWA8* can affect mitochondrial function in ARPE-19 cells. Electron microscopy showed that the mitochondria of cells in the control group were wrapped in the outer membrane and arranged in horizontal ridges, whereas the outer membrane of the mitochondria of cells in the *VWA8*-siRNA group were swollen, with the ridges damaged. Additionally, there was a decrease in the matrix electron density of cells in the *VWA8*-siRNA group (figure 5A, black arrows). Compared with the control group, there was a significant increase in the number of defective mitochondria in the *VWA8*-siRNA group (figure 5B). Additionally, mitochondrial permeability transition pore (mPTP) channels were opened in the siRNA group (figure 5C), with a decrease in the level of mitochondrial membrane potential (MMP) (figure 5D). Moreover, there was a significant increase in mitochondrial ROS production in the siRNA group (figure 5E,F). Seahorse assay was performed to further confirm the effect of *VWA8* deletion on mitochondrial respiratory function. Compared with the control group, there was a decrease in basal respiration, spare respiration capacity, maximal respiration and ATP production in the siRNA group (figure 5G). Transmission Electron Microscope (TEM) images showed a large accumulation of damaged mitochondria, and some of the damaged mitochondria were engulfed by a double membrane structure (figure 5A, red arrows). Therefore, we speculated that the increase in mitochondrial dysfunction may be related to abnormal mitochondrial autophagy. Additionally, western blotting showed that there was a marked increase in the expression of the autophagy marker microtubule-associated protein light chain 3 (LC3) in the siRNA group compared with that in the control group (figure 5H,I) and a decrease expression of P62 in the siRNA group (online supplemental figure S6). Colocalisation of LC3-stained autophagosomes and TOMM20-stained mitochondria in the *VWA8* siRNA group and the appropriate control group was analysed to determine increase in mitophagy in *VWA8*-deficient ARPE-19 cells.

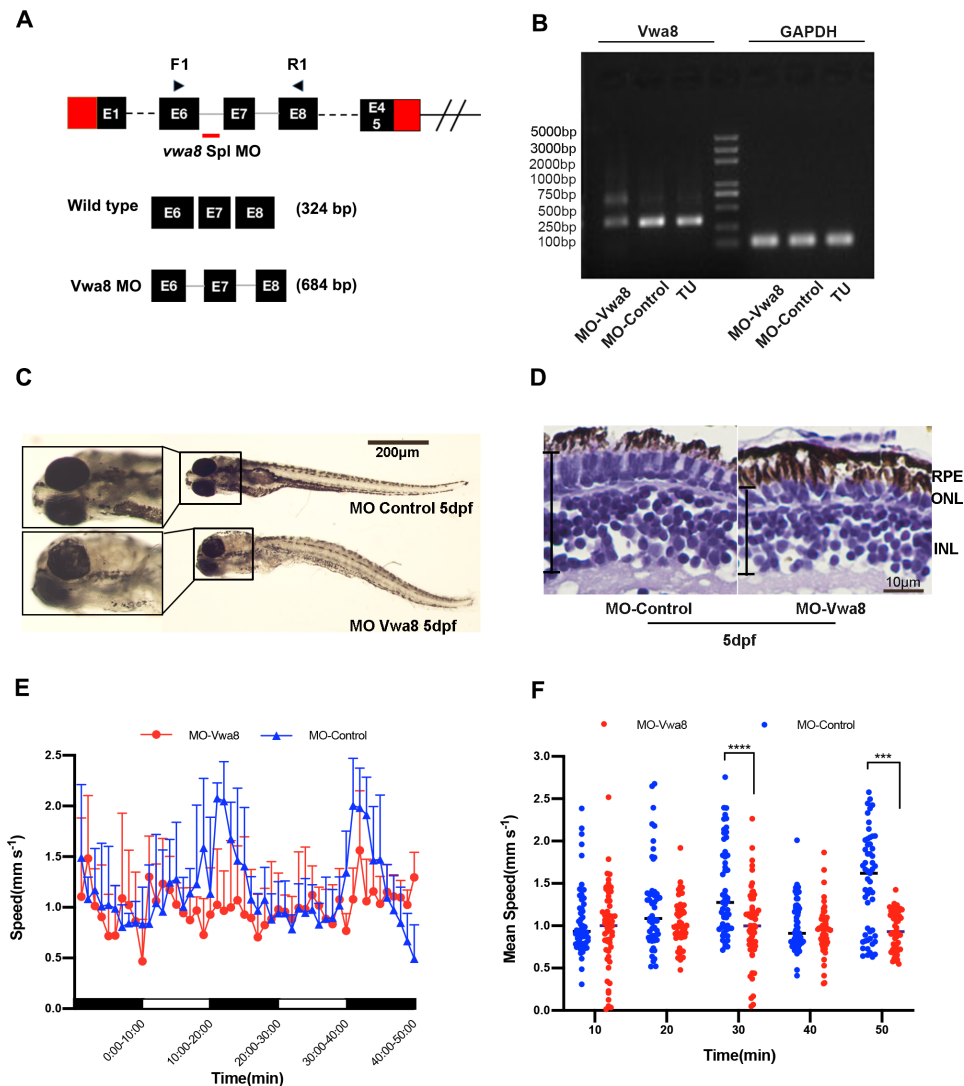


Figure 3 Knockdown of *Vwa8* in zebrafish. (A) Diagram showing *Vwa8*-MO knockdown mode; the exons of wild-type *Vwa8* E6–E8 were 324 bp fragments, and the splicing of *Vwa8* was induced by injecting of *Vwa8*-MO (4 ng), which resulted in 684 bp products. (B) Injection with *Vwa8*-MO significantly reduced *Vwa8* mRNA expression 5 dpf. *Vwa8* abnormal splice products at 684 bp were isolated from the *Vwa8*-MO group, indicating that the *Vwa8* knockdown zebrafish model was successfully constructed. (C) Compared with embryos injected with control-MO, embryos injected with *Vwa8*-MO 5 dpf showed abnormal eye pigmentation. Scale bar=200 μ m. (D) H&E staining revealed that the retinal ONL and INL (line area) were significantly narrower in embryos injected with *Vwa8*-MO at 5 dpf compared with embryos injected with control-MO. Scale bar=10 μ m. (E) Light-induced locomotor response with sudden light-to-dark transitions demonstrated significant dark adaptation impairment in zebrafish embryos injected with *Vwa8*-MO 5 dpf compared with embryo in the control group ($n=6$ per group). (F) Light-induced locomotor responses indicate significant differences in responses between *Vwa8*-MO and control-MO groups during the light-off phase ($n=10$ per group). **** $P<0.001$, *** $P<0.0001$ (Dunnett's t-test). dpf, days post fertilisation; INL, internuclear layer; MO, morpholino; ONL, outer nuclear layer; RPE, retinal pigment epithelium.

Consistent with the western blotting results, LC3 staining was stronger in the *VWA8*-siRNA group than in the control group (figure 5J,K). Furthermore, there was a higher level of LC3 puncta, with TOMM20-stained mitochondria in the *VWA8*-siRNA group, indicating activation of mitophagy. Moreover, cytochrome C expression was downregulated in the mitochondria of *VWA8*-siRNA-transfected ARPE-19 cells but significantly upregulated in the cytoplasm, indicating that silencing *VWA8* promoted the spilling of cytochrome C from the mitochondria into the cytoplasm, thereby activating the release of apoptotic factors (figure 5L,M). Additionally, a typical apoptotic nucleus morphology was observed in *VWA8*-deficient ARPE-19 cells, magnification means edge set of nuclear chromatin and condensed under the nuclear membrane (figure 5A). These results suggest

that silencing *VWA8* can induce mitochondrial dysfunction and promote mitophagy and apoptosis.

Decrease in *VWA8* expression activated cell apoptosis

An apoptosis-related assay was performed to determine whether ARPE-19 cell apoptosis was affected by a decrease in *VWA8* expression. The expression of apoptosis-related proteins, including cleaved-caspase 3 and 9, Bax and Bcl-2, was altered in the *VWA8*-siRNA group. Additionally, silencing *VWA8* promoted the expression of the pro-apoptotic proteins, including cleaved-caspase 3 and 9 and Bax, but suppressed the expression of the anti-apoptotic protein Bcl-2 (figure 6A–F). Flow cytometry (figure 6G,H) and TUNEL assay (figure 6I,J) confirmed that silencing *VWA8* promoted ARPE-19 cell apoptosis. Overall,

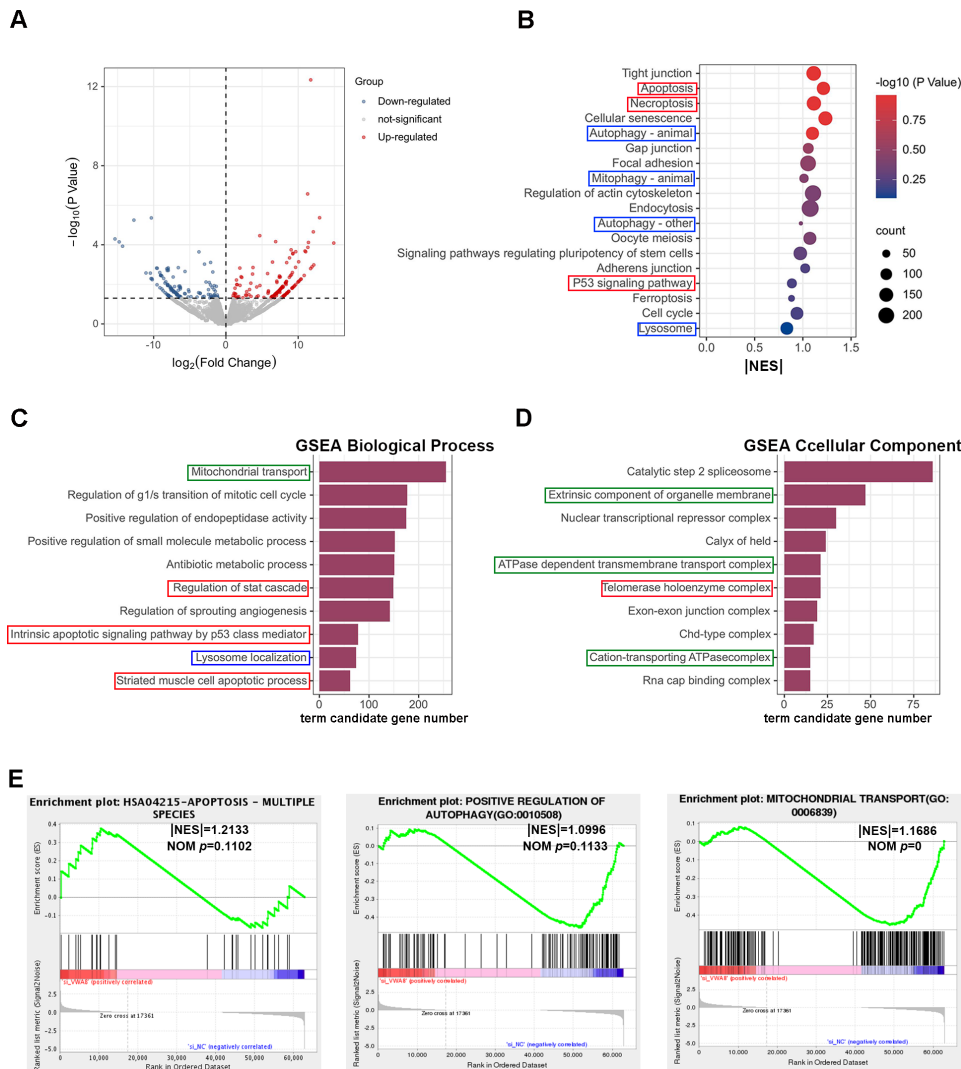


Figure 4 Transcriptome alterations in ARPE-19 cells transfected with *VWA8*-siRNA. (A) DEGs in *VWA8*-siRNA-treated and untreated ARPE-19 cells ($p \leq 0.05$). (B) The enriched Kyoto Encyclopaedia of Genes and Genomes (KEGG) pathway in cellular processes including apoptosis-related pathways (red rectangles) and autophagy-related pathways (blue rectangles). (C) Top 10 enriched terms in ‘biological process’ include apoptosis-related terms (red rectangles), autophagy-related terms (blue rectangles) and mitochondria-related terms (green rectangles). NOM $p < 0.05$, [NES] > 1 for all terms. (D) Top 10 enriched terms in ‘cellular components’ include apoptosis-related terms (red rectangle) and mitochondria-related terms (green rectangles). NOM $p < 0.05$, [NES] > 1 for all terms. (E) Apoptotic, autophagy and mitochondrial transport pathway enrichment plot. DEG, differentially expressed gene; GSEA, gene set enrichment analysis; NES, Normalised Enrichment Score; NOM, nominal; *VWA8*, von Willebrand factor A domain containing 8.

these results suggest that a decrease in *VWA8* expression induced cell apoptosis, resulting in cell degeneration.

DISCUSSION

RP is the most common hereditary retinopathy responsible for bilateral blindness and is caused by several genetic variants. Over the years, genetic analysis based on pedigree has facilitated the discovery of RP pathogenic genes,^{31 32} seeking new molecular diagnosis and gene therapy targets is considered a breakthrough of RP treatment. *VWA8*, a potential pathogenic gene, was identified in a 24-individual RP pedigree by exome sequencing, among which 11 family members were affected by adRP. It is rare to have such a large family with complete clinical data.^{33 34} Further analysis indicated that the 11 patients exhibited phenotypes consistent with that of RP, including macular dystrophy, macular degeneration and vitreous abnormality, and five patients exhibited dyslipidaemia. Genealogical characteristics suggested an ad inheritance pattern. A two-loci heterozygous mutation in *VWA8*

gene, c.3070G>A; c.4558C>T (p.Gly1024Arg; p.Arg1520Ter), was identified in the proband patient and confirmed in three other patients by exome sequencing. It should be noted that the variants we exclude cannot be completely excluded to be pathogenic, and these variants are not the focus of this study. Additionally, the variant was confirmed by Sanger sequencing in six patients. The variant was not observed with RP absent or rare in different publicly available online databases, such as gnomAD, ExAC, 1000 Genome, and ESP6500SI. A study by Aylward *et al* found that the p.Arg1520Ter variant of *VWA8* may be involved in non-syndromic cleft lip and palate (NSCLP), but it was not included in the final candidate variant due to the variant not completely segregating with NSCLP.³⁵ However, there is no report on the correlation between *VWA8* and retinal development.

Although it has been reported that *VWA8* is highly expressed in the mouse heart, kidney and liver and less expressed in the spleen, intestine and stomach,¹⁹ this is the first study to identify

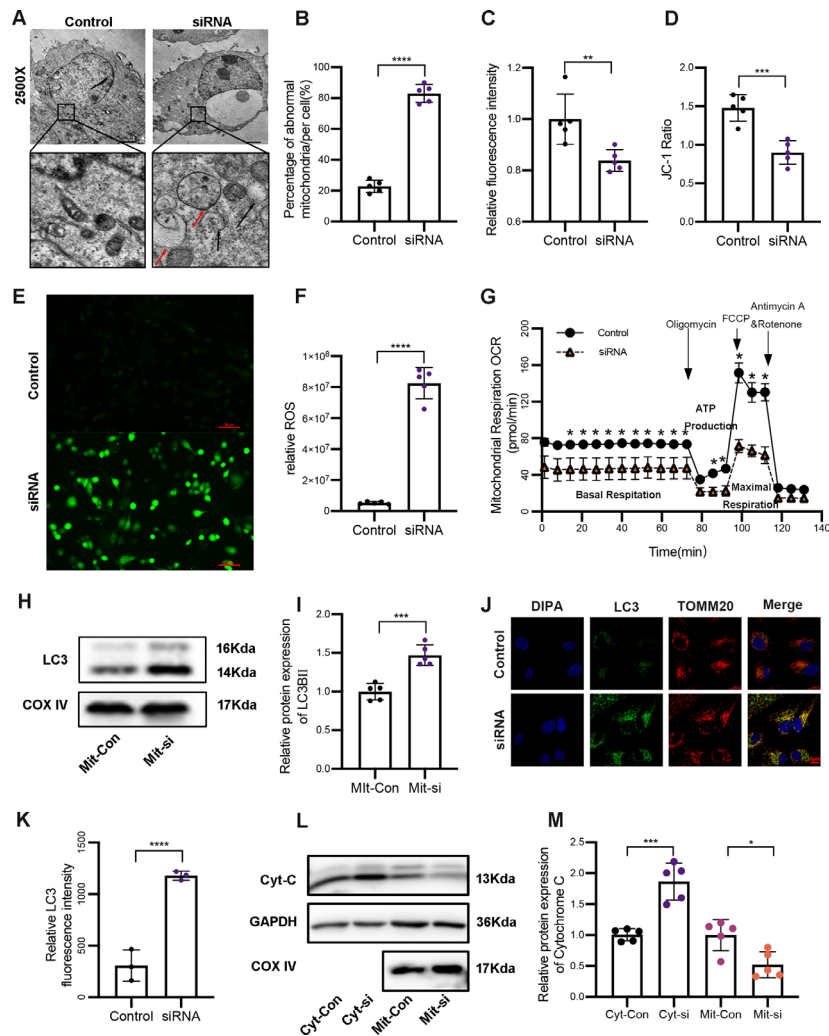


Figure 5 Mitophagy was activated by a decrease in *VWA8* expression. (A) TEM images of *VWA8*-siRNA-treated and untreated ARPE-19 cells. Black arrows indicate defective mitochondria with the swollen and deformed outer membrane, whereas red arrows represent autophagosomes surrounding the defective mitochondria. TEM image of siRNA cells shows typically condensed chromatin (scale bar=2 μ m). The lower left image is a digital magnification image of the black box area in the TEM image of the control group, and the lower right image is the digital magnification image of the black box area in the TEM image of the siRNA group. (B) Defective mitochondrial rates in ARPE-19 cells. Defective mitochondrial rate denotes number of defective mitochondria divided by total number of mitochondria (n=5, Student's t-test). (C) Histogram showing fluorescence intensity of calcein am. The weaker the fluorescence intensity, the higher the opening of the mPTP channel. Data are presented as the mean \pm SD of five independent experiments (n=5, Student's t-test). (D) Histogram showing the ratio of green fluorescence intensity to the red fluorescence intensity of JC-1. The degree of depolarisation of MMP is usually measured by the relative ratio of green to red fluorescence of the JC-1 probe. There was a decrease in the MMP of cells in the siRNA group compared with that of cells in the control group. Data are presented as the mean \pm SD of five independent experiments (n=5, Student's t-test). (E) Representative fluorescence intensity of *VWA8*-siRNA-treated and untreated ARPE-19 cells, indicating reactiveoxygenspecies (ROS) levels. The green fluorescence represents ROS production (scale bar=50 μ m). (F) Histogram of green fluorescence intensity of *VWA8*-siRNA-treated and untreated ARPE-19 cells. Cells in the siRNA group had higher ROS levels than cells in the control group. Data are presented as the mean \pm SD of five independent experiments (n=5, Student's t-test). (G) Seahorse analysis curve for ARPE-19 cells transfected with *VWA8* siRNA and control cells. Compared with the control group, the normalised OCR of the siRNA group showed a significant decrease in basal respiration, reserve respiration capacity, maximum respiration and ATP production. Data are presented as the mean \pm SD of five independent experiments (n=5, Student's t-test). (H) Representative western blot for LC3 expression in the mitochondria of *VWA8*-siRNA-treated and untreated ARPE-19 cells; Cox IV was used as a loading control. (I) Histogram showing the relative expression of LC3 protein in the mitochondria of *VWA8*-siRNA-treated and untreated ARPE-19 cells. The mitochondria of cells in the siRNA group had significantly higher expression of LC3 protein compared with cells in the control group. Data are presented as the mean \pm SD of five independent experiments (n=5, Student's t-test). (J) Immunofluorescence staining with LC3-labelled autophagosomes (green) and TOMM20-labelled mitochondria (red). The nuclei of *VWA8*-siRNA-treated and untreated ARPE-19 cells were counterstained with DAPI (blue) (scale bar=5 μ m). (K) Histogram showing the relative quantification of fluorescence intensities of *VWA8*-siRNA-treated and untreated ARPE-19 cells for LC3. Cells in the siRNA group had significantly higher expression of LC3 protein than cells in the control group. Data are presented as the mean \pm SD of five independent experiments (n=5, Student's t-test). (L) Representative western blot for cytochrome c protein in the mitochondria and cytoplasm of *VWA8*-siRNA-treated and untreated ARPE-19 cells. Cox IV and GAPDH were used as loading controls. (M) Histogram showing the relative expression of cytochrome c protein in the mitochondria and cytoplasm of *VWA8*-siRNA-treated and untreated ARPE-19 cells. There was a spillage of cytochrome c protein from the mitochondria to the cytoplasm in siRNA-treated cells. Data are presented as the mean \pm SD of five independent experiments (n=5, Student's t-test). *P<0.05, **P<0.01, ***P<0.001, ****P<0.0001. MMP, mitochondrial membrane potential; mPTP, mitochondrial permeability transition pore; *VWA8*, von Willebrand factor A domain containing 8.

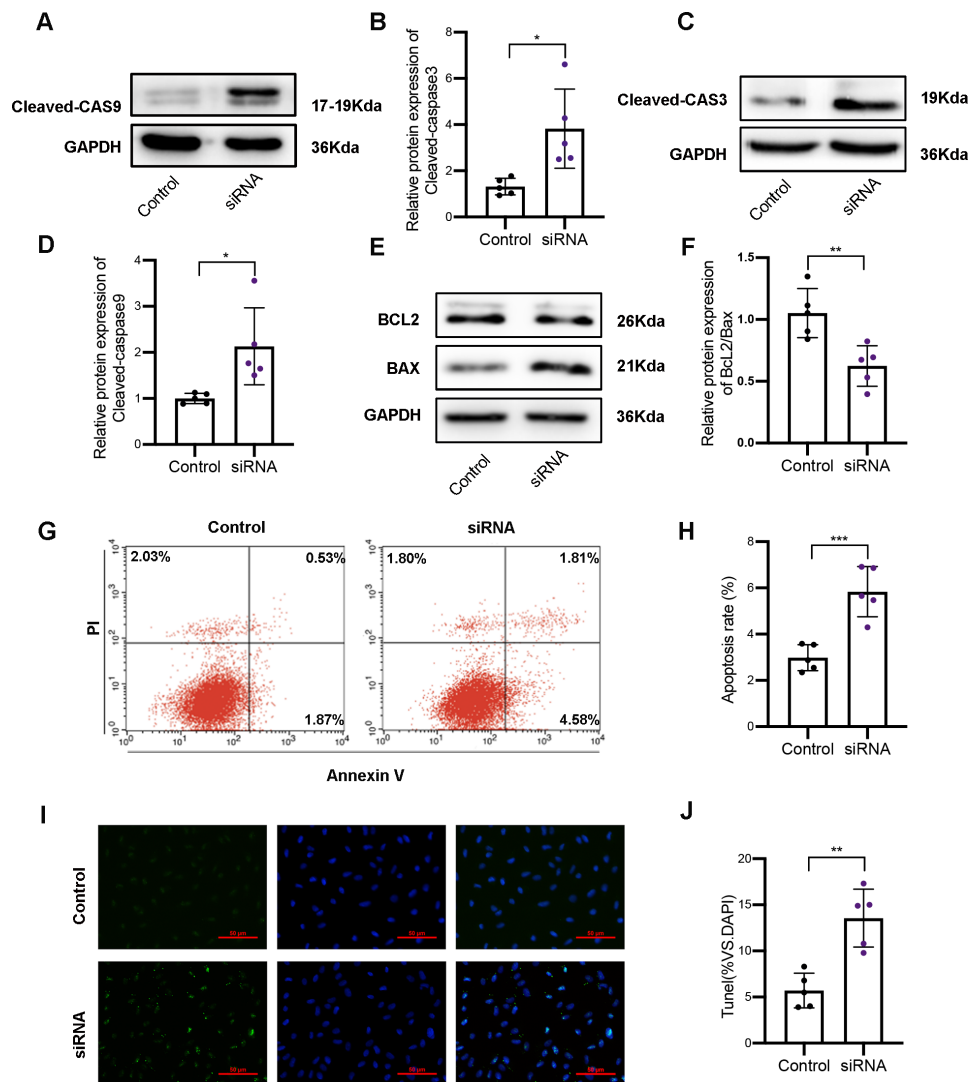


Figure 6 Decrease in *VWA8* expression-induced cell apoptosis. (A) Representative western blot of *VWA8*-siRNA-treated and untreated ARPE-19 cells for cleaved-caspase 9. (B) Histogram showing the relative expression of cleaved-caspase 9 protein in *VWA8*-siRNA-treated and untreated ARPE-19 cells. *VWA8*-siRNA-treated cells had significantly higher expression of cleaved-caspase 9 protein than untreated cells. Data are presented as the mean±SD of five independent experiments (n=5, Student's t-test). (C) Representative western blot of *VWA8*-siRNA-treated and untreated ARPE-19 cells for cleaved-caspase 3. (D) Histogram showing the relative expression of cleaved-caspase 3 protein in *VWA8*-siRNA-treated and untreated ARPE-19 cells. *VWA8*-siRNA-treated cells had significantly higher expression of cleaved-caspase 3 protein than untreated cells. Data are presented as the mean±SD of five independent experiments (n=5, Student's t-test). (E) Representative western blot of *VWA8*-siRNA-treated and untreated ARPE-19 cells for Bax and Bcl-2. (F) Histogram showing the ratio of Bcl-2 to Bax in *VWA8*-siRNA-treated and untreated ARPE-19 cells. *VWA8*-siRNA-treated cells had a significantly higher ratio of Bcl-2 to Bax than untreated cells. Data are presented as the mean±SD of five independent experiments (n=5, Student's t-test). (G) Flow cytometry assay of *VWA8*-siRNA-treated and untreated ARPE-19 cells. Cell apoptosis was determined using annexin V/PI double staining. (H) Histogram showing the apoptotic cell ratio of *VWA8*-siRNA-treated and untreated ARPE-19 cells. Data are presented as the mean±SD of five independent experiments (n = 5, Student's t-test). (I) TdT-mediated dUTP nick end labeling (TUNEL) assay was performed to determine DNA damage in *VWA8*-siRNA-treated and untreated ARPE-19 cells. Apoptotic cells were indicated by TUNEL reagent conjugated to green fluorescent Alexa fluor 488 dye (green), and nuclei were visualised by DAPI staining. Scale bar=50 µm. (J) Histogram showing the number of TUNEL reagent-stained cells. The *VWA8*-siRNA group had significantly higher numbers of apoptotic cells than the control group. Data are presented as the mean±SD of five independent experiments (n = 5, Student's t-test). *P<0.05, **P<0.01, ***P<0.001. *VWA8*, von Willebrand factor A domain containing 8.

VWA8 in eye tissues. The findings of the present study showed that *VWA8* is specifically expressed in the retina of fetal eye tissues but is rarely expressed in the sclera, cornea and lens, suggesting a potential link between *VWA8* and retinal disease. We identified a nonsense mutation (c.4558C>T (p.Arg1520Ter)) that is linked to a missense mutation (c.3070A>G (p.Gly1024Arg)) in the patients; the variant had the ability to escape NMD, and it is speculated that haploinsufficiency affected *VWA8* expression through early termination of translation. Knocking down

VWA8 significantly increased embryonic mortality in zebrafish, indicating that *VWA8* is critical for early embryo development. Additionally, the *VWA8* knockdown zebrafish model displayed the RP phenotype as individuals harbouring *VWA8* variants. These findings suggest that *VWA8* plays a significant role in early retinal development and could be a pathogenic gene for adRP.

Furthermore, the expression profiles of ARPE-19 cells transfected with *VWA8*-siRNA and untreated cells were examined by RNA sequencing and indicated that the gene sets were

significantly enriched in mitochondrial function, autophagy and apoptosis. Although it has been suggested that *VWA8* may be related to mitochondrial function, the specific effect and mechanism of *VWA8* deficiency on mitochondrial function still needs to be extensively studied. The findings of this study showed that silencing *VWA8* expression caused a decrease in cell MMP, induced the opening of mPTP channels, increased ROS accumulation and induced abnormal mitochondrial oxidative respiration. Additionally, TEM revealed that most mitochondrial ridges in *VWA8*-deficient RPE cells were damaged. Moreover, several studies have indicated the effect of autophagy regulation on RP.^{36–38} In the present study, mitochondrial defects activated autophagy, which enhanced autophagic flux, consequently inducing apoptosis. Cellular homeostasis plays an important role in maintaining cell activity, and an imbalance in cell homeostasis can impair cell function, leading to cell death. Studies on human and animal models of retinal dystrophy have suggested that apoptosis may be a common pathway for photoreceptor cell death.³⁹ It is crucial to find the molecular mechanism that causes the imbalance of autophagy and apoptosis homeostasis during retinal cell development. We identified for the first time the function of *VWA8* in regulating autophagy and apoptosis. Studies have shown that autophagy may initiate apoptosis.³⁹ The results of this study showed that there was an increase in LC3-II (a marker of autophagosomes) expression, and the expression of apoptosis markers, including caspase 3 and 9 and Bax in *VWA8*-deficient cells. Therefore, it could be included that *VWA8* deficiency can enhance autophagy flux and aggravate RPE cell apoptosis, thereby disrupting cellular homeostasis required for the development and survival of the retina.

VWA8 was identified in the human retina for the first time, filling the blank of the *VWA8* expression map in eye tissue, paving the way for future research on the specific roles of *VWA8* in ophthalmic diseases. Furthermore, the findings of this study showed that *VWA8* variants are likely loss of function variants that can induce mitochondrial defects, resulting in the activation of mitophagy and apoptosis, and consequently in RPE cell death. However, the specific mechanisms by which *VWA8* variants induce mitochondrial damage are yet to be clarified, indicating the need for further studies. Knocking down *VWA8* induced visual dysfunction in zebrafish, indicating the importance of *VWA8* in retinal development and survival. However, further studies need to be validated in other animal models and a large sample of patients with RP. The findings of this study showed that *VWA8* could be a key molecule for RP prenatal screening and a potential therapeutic target for RP treatment and provides a reference value for the study of other neurodegenerative diseases.

Acknowledgements We thank patients and their families for their participation, as well as YH and HH.

Contributors ZY conceived the project, designed the experiments and supervised the study. ZY is responsible for all contents as guarantor. RH revised the manuscript. LK designed and performed the experiments, analysed the data, and drafted the manuscript and figures. GC collected information on retinitis pigmentosa family. WM and JL assisted in the animal model preparation and sample collection. XW, HG, DL, WL, SC, SJ, YH and QL assisted in the preparation of the manuscript. XZ assisted in exome sequencing data analysis. All authors read and approved the final manuscript.

Funding This work was supported by the National Key Research and Development Program (2021YFC2701104 and 2021YFC2701003), the National Natural Science Foundation of China (grant numbers 82171649, 81871219 and 82271730) and Liaoning Revitalization Talents Program (XLYC1902099)

Competing interests None declared.

Patient consent for publication Not applicable.

Ethics approval This study involves human participants and all experiments were approved by the ethics committee of Shengjing Hospital affiliated with China Medical University (approval number 2019PS415K). This study conformed to the tenets of the Declaration of Helsinki. Written informed consent was obtained from all participants or their parents, on behalf of minors/child participants, prior to their inclusion in this study.

Provenance and peer review Not commissioned; externally peer reviewed.

Data availability statement All data relevant to the study are included in the article or uploaded as supplementary information.

Supplemental material This content has been supplied by the author(s). It has not been vetted by BMJ Publishing Group Limited (BMJ) and may not have been peer-reviewed. Any opinions or recommendations discussed are solely those of the author(s) and are not endorsed by BMJ. BMJ disclaims all liability and responsibility arising from any reliance placed on the content. Where the content includes any translated material, BMJ does not warrant the accuracy and reliability of the translations (including but not limited to local regulations, clinical guidelines, terminology, drug names and drug dosages), and is not responsible for any error and/or omissions arising from translation and adaptation or otherwise.

ORCID iD

Zhengwei Yuan <http://orcid.org/0000-0003-0967-9462>

REFERENCES

- Haim M. The epidemiology of retinitis pigmentosa in Denmark. *Acta Ophthalmol Scand Suppl* 2002;80:1–34.
- Wright AF, Chakarova CF, Abd El-Aziz MM, et al. Photoreceptor degeneration: genetic and mechanistic dissection of a complex trait. *Nat Rev Genet* 2010;11:273–84.
- Jayakody SA, Gonzalez-Cordero A, Ali RR, et al. Cellular strategies for retinal repair by photoreceptor replacement. *Prog Retin Eye Res* 2015;46:31–66.
- Birch DG, Bennett LD, Duncan JL, et al. Long-term follow-up of patients with retinitis pigmentosa receiving intraocular ciliary neurotrophic factor implants. *Am J Ophthalmol* 2016;170:10–4.
- Auricchio A, Smith AJ, Ali RR. The future looks brighter after 25 years of retinal gene therapy. *Hum Gene Ther* 2017;28:982–7.
- Murray SF, Jazayeri A, Matthes MT, et al. Allele-specific inhibition of rhodopsin with an antisense oligonucleotide slows photoreceptor cell degeneration. *Invest Ophthalmol Vis Sci* 2015;56:6362–75.
- Meng D, Ragi SD, Tsang SH. Therapy in rhodopsin-mediated autosomal dominant retinitis pigmentosa. *Mol Ther* 2020;28:2139–49.
- Colombo L, Maltese PE, Castori M, et al. Molecular epidemiology in 591 Italian probands with nonsyndromic retinitis pigmentosa and usher syndrome. *Invest Ophthalmol Vis Sci* 2021;62:13.
- Gao F-J, Li J-K, Chen H, et al. Genetic and clinical findings in a large cohort of Chinese patients with suspected retinitis pigmentosa. *Ophthalmology* 2019;126:1549–56.
- Murakami Y, Nakabeppu Y, Sonoda K-H. Oxidative stress and microglial response in retinitis pigmentosa. *Int J Mol Sci* 2020;21:7170.
- Wang F, Xu C, Reece EA, et al. Protein kinase C- α suppresses autophagy and induces neural tube defects via mir-129-2 in diabetic pregnancy. *Nat Commun* 2017;8:15182.
- Qiu Y-H, Zhang T-S, Wang X-W, et al. Mitochondria autophagy: a potential target for cancer therapy. *J Drug Target* 2021;29:576–91.
- Xu G, Li T, Chen J, et al. Autosomal dominant retinitis pigmentosa-associated gene PRPF8 is essential for hypoxia-induced mitophagy through regulating ULK1 mRNA splicing. *Autophagy* 2018;14:1818–30.
- Onishi M, Yamano K, Sato M, et al. Molecular mechanisms and physiological functions of mitophagy. *EMBO J* 2021;40:e104705.
- Scorrano L, Ashiya M, Buttle K, et al. A distinct pathway remodels mitochondrial cristae and mobilizes cytochrome C during apoptosis. *Dev Cell* 2002;2:55–67.
- Yang Y, Li Z-X, Hu X-M, et al. Insight into crosstalk between mitophagy and apoptosis/necroptosis: mechanisms and clinical applications in ischemic stroke. *Curr Med Sci* 2022;42:237–48.
- Pan M, Yin Y, Wang X, et al. Mice deficient in UXT exhibit retinitis pigmentosa-like features via aberrant autophagy activation. *Autophagy* 2021;17:1873–88.
- Luo M, Mengos AE, Ma W, et al. Characterization of the novel protein KIAA0564 (von willebrand domain-containing protein 8). *Biochem Biophys Res Commun* 2017;487:545–51.
- Grewe BS, Richmond JE, Featherstone DE. The spatial and developmental expression of mouse *vwa8* (von willebrand domain-containing protein 8). *Gene Expr Patterns* 2018;29:39–46.
- Anney R, Klei L, Pinto D, et al. A genome-wide scan for common alleles affecting risk for autism. *Hum Mol Genet* 2010;19:4072–82.
- Oedegaard KJ, Greenwood TA, Johansson S, et al. A genome-wide association study of bipolar disorder and comorbid migraine. *Genes Brain Behav* 2010;9:673–80.
- Newbury AJ, Rosen GD. Genetic, morphometric, and behavioral factors linked to the midsagittal area of the corpus callosum. *Front Genet* 2012;3:91.

- 23 Umair M, Farooq Khan M, Aldrees M, *et al.* Mutated *wva8* is associated with developmental delay, microcephaly, and scoliosis and plays a novel role in early development and skeletal morphogenesis in zebrafish. *Front Cell Dev Biol* 2021;9:736960.
- 24 Davalos V, Garcia-Prieto CA, Ferrer G, *et al.* Epigenetic profiling linked to multisystem inflammatory syndrome in children (MIS-C): a multicenter, retrospective study. *EClinicalMedicine* 2022;50:101515.
- 25 Wang Y, Chen S, Chen J, *et al.* Germline genetic patterns underlying familial rheumatoid arthritis, systemic lupus erythematosus and primary sjögren's syndrome highlight T cell-initiated autoimmunity. *Ann Rheum Dis* 2020;79:268–75.
- 26 Luo M, Willis WT, Coletta DK, *et al.* Deletion of the mitochondrial protein VWA8 induces oxidative stress and an HNF4 α compensatory response in hepatocytes. *Biochemistry* 2019;58:4983–96.
- 27 Wang R, Wang W-Q, Li X-Q, *et al.* A novel variant in FOXC1 associated with atypical axenfeld-rieger syndrome. *BMC Med Genomics* 2021;14:277.
- 28 van Dijk M, Mulders J, Poutsma A, *et al.* Maternal segregation of the dutch preeclampsia locus at 10q22 with a new member of the winged helix gene family. *Nat Genet* 2005;37:514–9.
- 29 Hendrickson A, Bumsted-O'Brien K, Natoli R, *et al.* Rod photoreceptor differentiation in fetal and infant human retina. *Exp Eye Res* 2008;87:415–26.
- 30 Luty GA, McLeod DS. Development of the hyaloid, choroidal and retinal vasculatures in the fetal human eye. *Prog Retin Eye Res* 2018;62:58–76.
- 31 Al-Khersan H, Shah KP, Jung SC, *et al.* A novel MERTK mutation causing retinitis pigmentosa. *Graefes Arch Clin Exp Ophthalmol* 2017;255:1613–9.
- 32 Arno G, Agrawal SA, Eblimit A, *et al.* Mutations in REEP6 cause autosomal-recessive retinitis pigmentosa. *Am J Hum Genet* 2016;99:1305–15.
- 33 Friedman JS, Ray JW, Waseem N, *et al.* Mutations in a BTB-kelch protein, KLHL7, cause autosomal-dominant retinitis pigmentosa. *Am J Hum Genet* 2009;84:792–800.
- 34 Dryja TP, McGee TL, Hahn LB, *et al.* Mutations within the rhodopsin gene in patients with autosomal dominant retinitis pigmentosa. *N Engl J Med* 1990;323:1302–7.
- 35 Aylward A, Cai Y, Lee A, *et al.* Using whole exome sequencing to identify candidate genes with rare variants in nonsyndromic cleft lip and palate. *Genet Epidemiol* 2016;40:432–41.
- 36 Yao J, Qiu Y, Frontera E, *et al.* Inhibiting autophagy reduces retinal degeneration caused by protein misfolding. *Autophagy* 2018;14:1226–38.
- 37 Boya P, Esteban-Martínez L, Serrano-Puebla A, *et al.* Autophagy in the eye: development, degeneration, and aging. *Prog Retin Eye Res* 2016;55:206–45.
- 38 Mathew B, Chennakesavalu M, Sharma M, *et al.* Autophagy and post-ischemic conditioning in retinal ischemia. *Autophagy* 2021;17:1479–99.
- 39 Kunchithapatham K, Rohrer B. Apoptosis and autophagy in photoreceptors exposed to oxidative stress. *Autophagy* 2007;3:433–41.